PROCESSING OF SIMRAD EM12 SONAR DATA FROM THE MID-ATLANTIC RIDGE (45°30'N)

Jane A Keeton and Roger C Searle

Department of Geological Sciences, University of Durham, South Road, Durham DH1 3LE, UK.

1. INTRODUCTION

The SIMRAD EM12 multibeam survey is sited at 45°30'N on the axis of the Mid-Atlantic Ridge (MAR). This area formed the basis for detailed geophysical work in the 1960s [1], later followed by the collection of GLORIA long range sidescan sonar data [2]. The EM12 survey was undertaken in December 1990, encompassing some 3000km^2, aboard the R/V Ocean Surveyor, operated by Worldwide Ocean Surveying Ltd. [3]. We present details of the data processing techniques developed to process the EM12 sidescan sonar data and a brief summary of the backscatter strength dependence on grazing angle, with particular relation to the geology of the area.

2. SIMRAD EM12 MULTIBEAM ECHOSOUNDER: THEORY OF OPERATION

The EM12 is a member of a new generation of multibeam echosounders operating at 13 kHz, with a coverage sector of 90° comprising 81 beams, a beam spacing of 1.1° and a vertical resolution of 2.4m. The EM12 detects the sea bottom using a combination of amplitude and phase information of the returned acoustic signal. The system has the ability to place the backscattered energy for each beam sample in its exact horizontal position on the seabed, thus producing a geometrically correct sidescan sonar image of the seafloor, co-registered with the bathymetry data [4].

The fundamental sonar equation for an echosounder is defined as: **EL = SL - 2TL + BS** where **EL** is the received echo level, **SL** the transmitter source level, **2TL** the two way transmission loss (in dB) and **BS** the backscattering strength of the target [5]. The transmission loss (in dB) is related to the range **R** and absorption coefficient α by: **2TL = 2αR + 40 log R**. Lambert's Law has often been used to describe the backscattering function with varying grazing angle θ_g and the non-angular dependent scattering coefficient μ: **BS = 10 log μ + 10 log sin^2 θ_g** [5]. The EM12 outputs backscatter values (**BS**) compensated for the source level (**SL**), the absorption coefficient (α) and the angular variation assuming a flat bottom. The latter correction removes the Lambert's Law effect for all grazing angles relative to a horizontal seafloor, this principle isclarified in section 6.2, where the effective resulting grazing angles are computed.

3. DATA ACQUISITION

The EM12 operated with a pulse length of 10ms and a ping rate of around 500 pings per hour. When surveying began in the north east of the area, there was a Force 8 gale blowing and the average ship speed was only 4-5 knots; conditions improved for the western region, where a speed of 10-11 knots was achieved. GPS navigation was available for 23.5 hours per day.

The EM12 system archives data on optical disks in the form of telegrams. The bathymetry data were processed on board ship using IRAP processing package [6], although further post-cruise editing was required due to excessive noise in the data [3]. The three forms of bathymetry data produced were the raw telegrams; ungridded 'xyz' files, following combination with navigation information held in position telegrams; and a digital grid generated from the edited 'xyz' files using GMT [7]. Navigation and depth telegram data were converted to a directly accessible format in day-long files. The sidescan data were available in their raw telegram format, with each telegram comprising around one hour's worth of data with approximately 500 samples per ping and being about 1 Mbyte in size. Amplitude samples are measured in dB and are located in metres relative to the ping origin.

4. SIDESCAN DATA PROCESSING

4.1 Telegram to image conversion

Each sidescan telegram is converted into both a tile and a geometrically correct image. For both image types, the UTM coordinates are determined for each ping origin through merging with the navigation files. The tile image origin is located at the centre beam of the first ping and all backscatter samples are measured in dB and located in metres from it. The distance between pings is determined according to how far the ship has travelled. This format is chosen particularly for ease in later quantitative analysis, where properties such as across-track profiles are important (see fig. 1). The geometric images are generated for mosaicking purposes. The position and heading for each ping origin are used to interpolate the UTM coordinates for all backscatter samples; the resulting ungridded 'xyz' files comprise backscatter strength measured in dB, each with UTM northings and eastings. An example is illustrated in fig. 2.

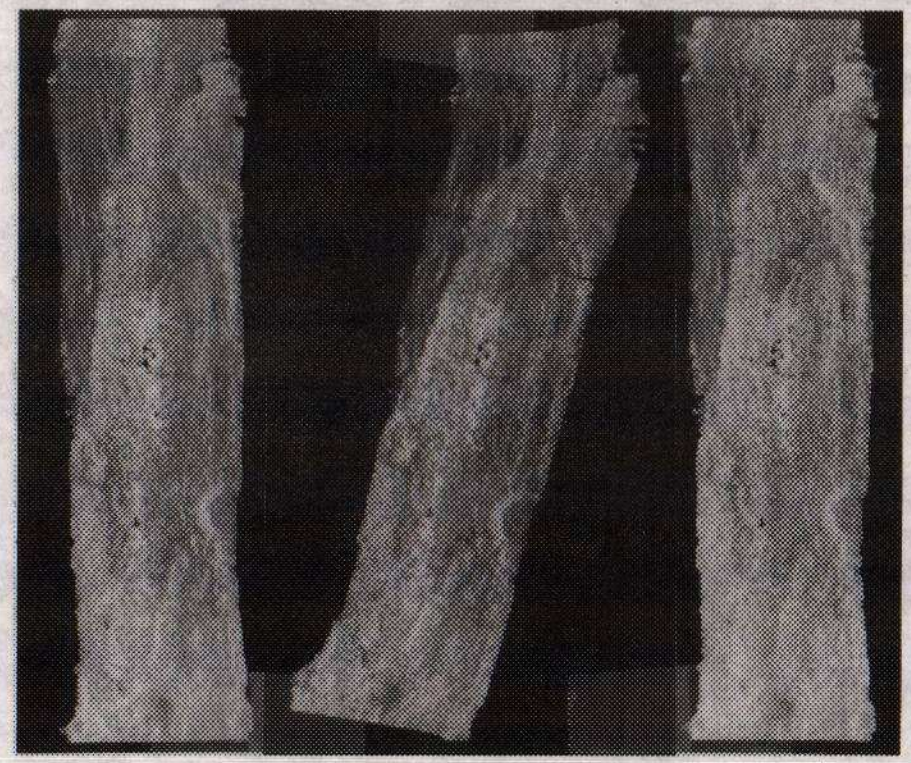

From left to right: ***figures 1, 2*** *and* ***3****, respectively displaying: (1) tile image without empirical beam correction (width ~6.3km, length ~21.6km), (2) geometrically correct image (width ~11.2km, length ~ 22.0km) and (3) tile image with correction applied. White corresponds to a backscatter strength of -0.5dB, black to -64.0dB. The tiles are oriented with the most recent ping at the bottom of the image, port returns on the left and starboard on the right.*

One tile and one geometric 'xyz' file is generated from each sidescan telegram; these files are gridded and the backscatter values are linearly compressed from 32 to 8 bits. The gridding routine employed is 'GINTP1' from UNIRAS. The 'xyz' data are binned to their closest grid nodes, and double linear interpolation fills in some of the gaps. A 36m cell size is selected here, and a search radius of 72m. Header information is retained in separate files.

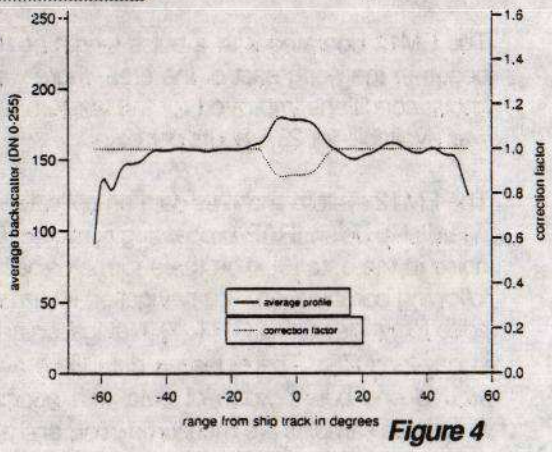

Figure 4

4.2 Derivation of Empirical Beam Pattern

Although the sidescan telegrams provided by the EM12 are already corrected for beam effects, due to the nature of sidescan performance and the invalidity of the first order Lambert's Law

correction at small beam angles, the inner 20° near-nadir of the swath remain unreliable, leaving a bright stripe down the centre of the image (fig. 1). An attempt has been made to reduce this 'stripe', purely for aesthetic purposes, in order to reduce the visual distraction of the artifact from the actual data in the final mosaic. The remaining 'beam pattern' is derived through the selection of average across-track profiles generated from 6 of the best quality sidescan tiles, representing 10% of the total number. A simple correction function, displayed in fig. 4, is determined by combining these profiles, averaging and filtering. This function is applied during the processing of all sidescan images, fig. 3 illustrates the result of applying the correction to the sidescan tile in fig. 1.

4.3 Mosaicking

This procedure utilises the geometric images and EASIPACE software. A basemap is generated, onto which the images are placed, according to their UTM limits. For overlapping swaths, the whole process can be performed automatically and quickly with the most recent swath always overlaying the previous adjacent one, or vice versa. However, due to the poor quality of the dataset used here, it was essential to manually define a 'cut line' between two overlapping swaths through an assessment of data quality and clarity of features. This procedure takes significantly longer.

5. RESULTS

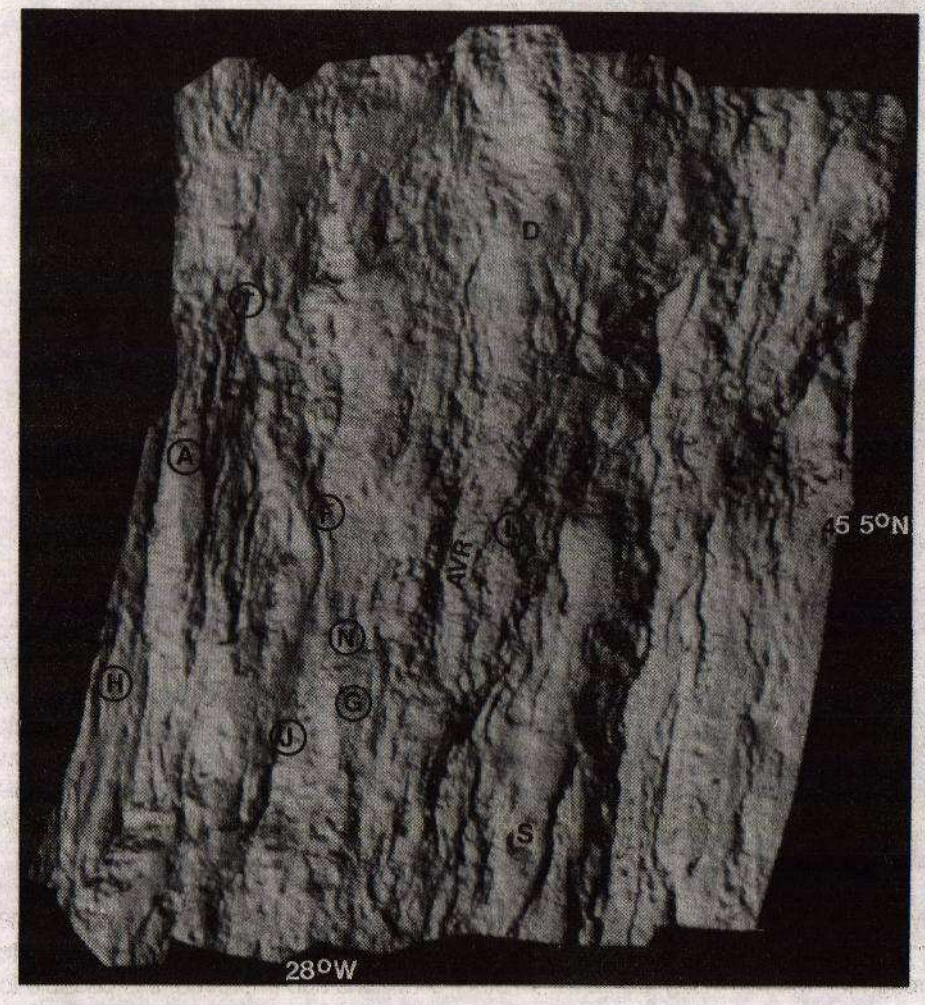

Figure 5: *a shaded relief image generated from the bathymetry, with illumination from the north east. This, and all subsequent whole area images, have UTM bounds: NW 400000E, 5075000N; SE 470000E, 5005000N. This is approximately 70x70km.*

EM12 SONAR PROCESSING

5.1 Geology

The slow spreading (1cm/year half spreading rate) MAR axis at 45°30'N is expressed as a median valley, striking 020°, between 8.5 and 22km wide and approximately 3km deep. Axial volcanic ridges (AVRs) can be identified on the valley floor, striking obliquely to the median valley at 010°. The ridges are right-laterally offset and the offset regions are characterised by structural depressions (D). The remains of ancient volcanic ridges (J, T, H) and depressions (A) can be clearly traced off axis. Individual circular volcanic seamounts are observed on the valley floor (S). The median valley walls rise by between 0.3-1km and sometimes comprise multiple parallel fault scarps (L). These median valley parallel faults extend throughout the survey area, principally inward facing, although a small proportion are outward facing. Numerous landslides have been identified from the morphology of some of these scarps (N). With regard to lithology [1], the AVRs would be composed of freshly formed basalt, with structural depressions forming pockets of sediments and sediment thickness increasing with distance from the ridge axis. Fault scarp exposures can yield more massive gabbroic fabrics.

5.2 Sidescan Data Description

Figure 6 *illustrates the complete SIMRAD sidescan mosaic; the survey lines run approximately NNE to SSW. Black represents low backscatter (-64dB) while white corresponds with high backscatter (-0.5dB).*

Unfortunately, the data quality clearly suffers due to poor weather conditions, particularly in the eastern region. The loss in quality of the data is most noticeably expressed as complete 'holes' in the mosaic where we were unable to pick up any returns. Even through the median valley where the weather conditions had improved, it is possible to

identify in which direction the ship was steaming, with rougher conditions resulting in generally 'darker' swaths where the signal has been attenuated due to aeration around the transducer faces. Through comparison with the bathymetry data, a broadly bright distribution of pixels is associated with the median valley, representing the high backscattering properties of rough basaltic terrain. The small seamounts are picked out well. Elongated bands of high backscattering pixels coincide with many of the fault scarps, particularly the multiple faulting in the south eastern median valley wall. The backscatter generally decreases with increasing distance from the ridge axis and structural depressions clearly exhibit the lowest backscatter values.

6. RELATIONSHIPS BETWEEN ACOUSTIC BACKSCATTER AND GEOLOGY

6.1 Previous Work

A relationship has been identified by many workers between backscatter (BS) and bottom type, generally with high BS for rocks and low for sediments, together with a Lambertian dependence between BS and grazing angles below ~45° [8]. These phenomena have been physically modelled, deducing that bottom roughness also considerably affects the BS return [9]. Recently, investigations have yielded a similar angular dependence of BS strength for Seabeam 12 kHz data over sediments [10] and GLORIA 6 kHz sidescan sonar data over a mid-ocean ridge [11].

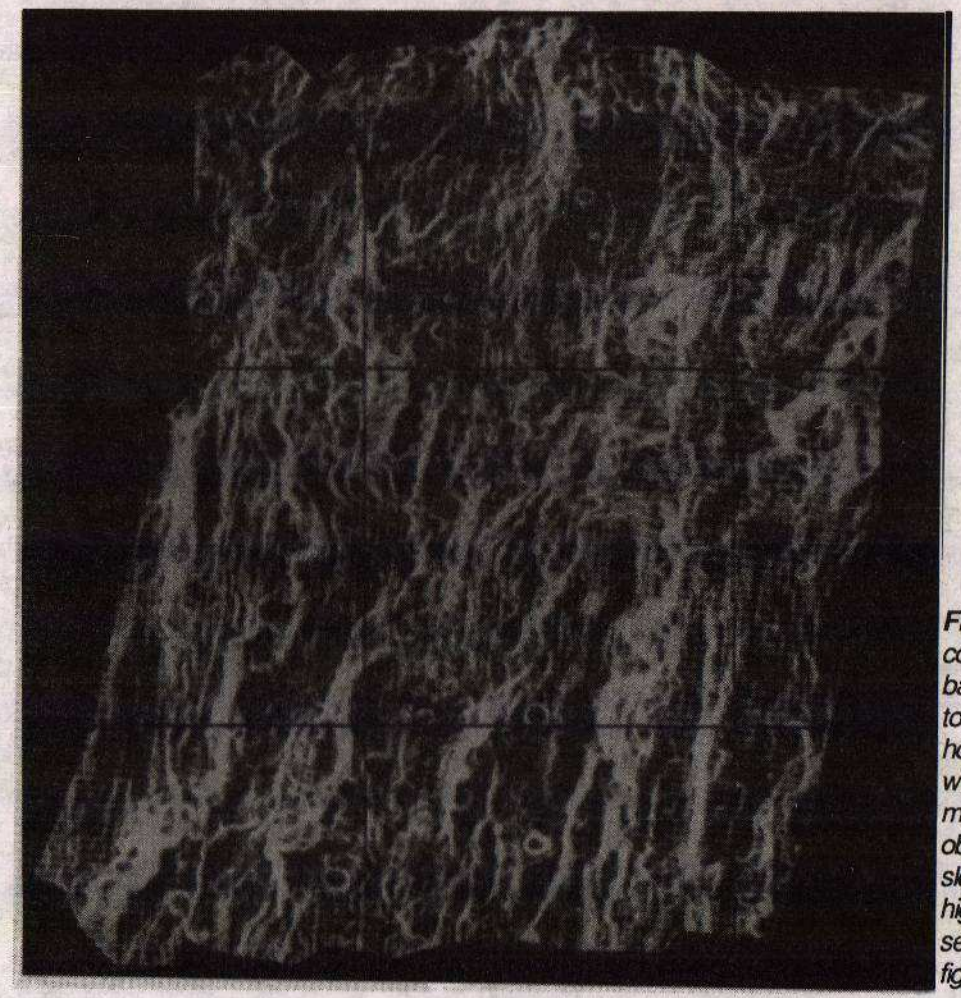

***Figure 7**: the grazing angles computed from the bathymetry grid, black refers to an angle of 90° (i.e. horizontal seafloor), while white corresponds to the minimum grazing angle observed of 24° (a seafloor slope of 66°). This image highlights the fault scarps and seamounts identified in earlier figures.*

EM12 SONAR PROCESSING

6.2 Grazing Angle Computation

Since the EM12 backscatter strengths, as recorded, have been corrected for Lambert's Law assuming a flat seafloor, that is, the backscatter variation due to the beam angle has been removed. In effect, if the scattering is purely Lambertian, the data are as they would have been recorded with a vertically incident beam. Therefore, the angle of incidence is defined as the angle between the normal vector to the seafloor surface and the vertical, while the grazing angle is the complement of this (see figs. 7 & 8).

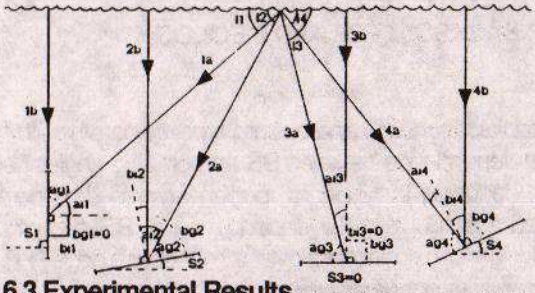

Figure 8 illustrates four examples of the grazing angle definition. In each example, case 'a' refers to the conventional grazing angle for a sidescan sonar, while case 'b' corresponds with the situation we have here. The letter 'i' denotes angles of incidence, 'g', grazing angles, 'S', the slope of the seafloor (in 2 dimensions rather than the 3 actually used) and 'l', the beam angle.

6.3 Experimental Results

The dependence of acoustic BS strength on grazing angle (θ_g) for the entire survey area is illustrated in fig. 9, with some basic statistics in table I. The distribution is somewhat skewed towards higher BS returns for lower θ_g, this contradicts the Lambertian distribution observed in previous work. This skew may be explained by the fact that mid-ocean ridges are partly characterised by highly faulted terrain; where these steep, low θ_g fault scarps may be composed of material with an intrinsically higher BS strength than the flat, high θ_g material in between.

The BS/θ_g relationship has been investigated for a number of geological settings, selected purely according to their bathymetric situation. We shall not attempt to explain the relationships acoustically, rather to present some typical results and relate them to the geology. Fig. 5 locates the experimental sites, fig. 10 presents the backscatter/grazing angle results and table I summarizes some basic statistics from each site.

Two of the lithologically most diverse terrain types are the AVR and sedimented basin found at G and A, respectively. Both sites exhibit a relatively small range of both backscatter strength and grazing angle; the principle difference between the two is the modal BS value. The landslide, N, possesses slightly lower BS strengths than the median valley floor, but a larger θ_g variation which could be attributed to its inherent slope. The median valley bounding fault at L is composed of multiple scarps where BS sharply increases towards lower θ_g (fault scarps) with higher θ_g related to the sedimented areas in between. The BS dependence on θ_g for the faults at location F appears to be more closely related to the landslide at N rather than the faults of L, maybe this scarp is draped with talus.

ID	BS mode	Min BS	Max BS	θg mode	Min θg	Max θg	Skew
entire survey area	-30	-64	-0.5	82	24	90	slight *
G - med. valley ridge(1)	-22	-33	-12	85	70	90	none
J - off axis ridge (2)	-24	-35	-15	72	50	88	none
T - off axis ridge (3)	-23	-40	-10	65	30	90	complex
H - off axis ridge (4)	-30	-39	-18	85	75	90	none
A - sedimented basin	-37	-45	-25	86	80	90	none
N - landslide	-25	-34	-18	77	56	85	none
F - fault scarps	-30	-39	-18	83	60	90	slight *
L - fault scarps	-20	-40	-08	70	56	90	sharp *

* denotes increased backscatter strength with decreasing grazing angle

Table I

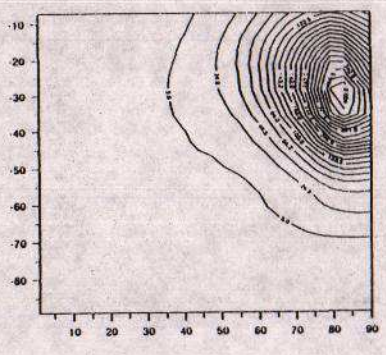

***Figure 9:** BS/θg plot for whole survey area, contours represent 1dB/1° bins.*

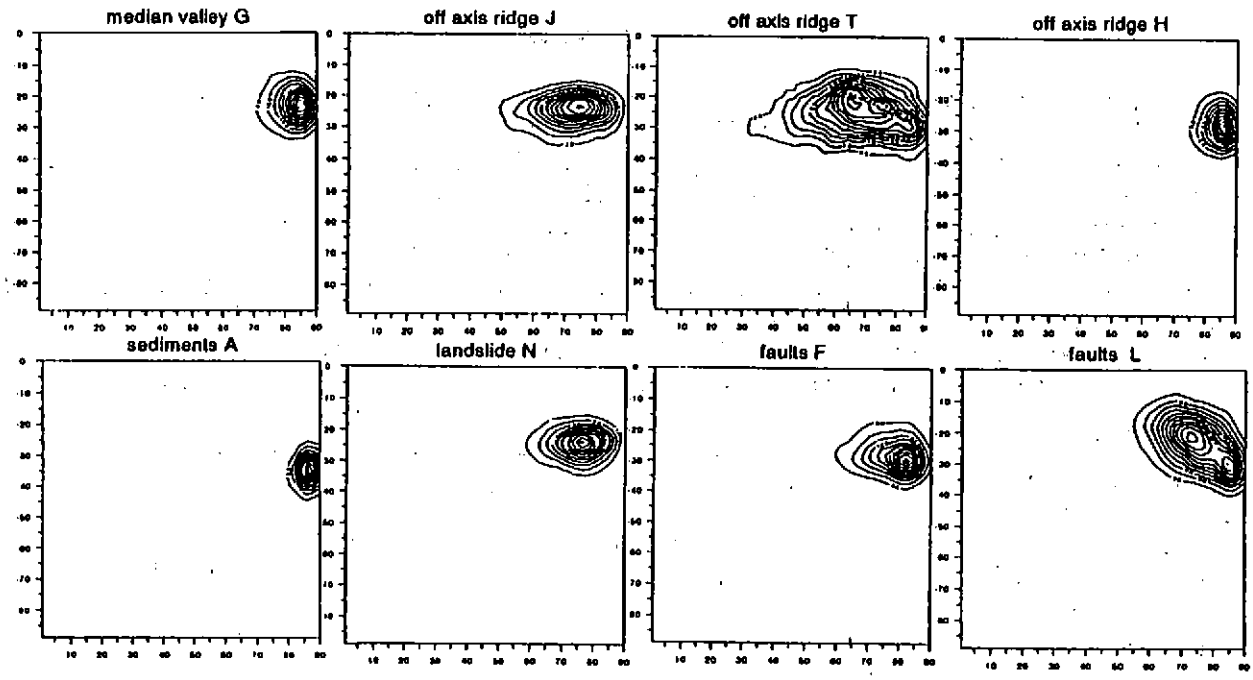

Figure 10: BS/θg plots for selected sites, again contours represent 1dB/1° bins.

Of particular interest is the backscatter/grazing angle relationship of G, J, T and H, corresponding with volcanic ridges at increasing distances from the ridge axis (respectively 0, 7, 17 & 19km). A typical scenario through time for such ridges would involve a freshly erupted basaltic AVR, increasingly faulted with time due to lithospheric extension, concurrent with increased sedimentation. Eventually, this faulting ceases and the rocks become totally buried by sediments [12]. The backscatter/grazing angle plots in fig. 10 appear to relate to this geological theme. G comprises closely packed high backscatter and grazing angles; J has an overall lower backscatter strength with a larger range of grazing angles, related to the initiation of faulting; T possesses a very broad distribution of both backscatter and grazing angles, suggesting increased faulting and sedimentation; ridge H exhibits the lowest backscatter strength of the selection and small ranges of both parameters. At T, backscatter increases with grazing angle below about 65°, then decreases again with lower grazing angle. The initial high grazing angle skew may be explained by interspersed fault and sediment fabrics, but once slopes of greater than 25° are attained, only uniformly Lambertian scattering fault scarps would remain. No fault-like backscatter skew with grazing angle is obvious at ridge H; so we propose that the fault scarps no longer breach the sediments. Also, the backscatter strength here is still higher than the sedimented basin in A, suggesting the sediment blanket over the ridge is thinner than in the basin.

7. CONCLUSIONS

The processing of EM12 sidescan data has been developed, resulting in a geometrically correct mosaic. The backscatter strength and grazing angle can be characterised qualitatively for geological terrains, although the overall aim of the exercise would be to provide an automatic geological classification. Simple quantitative classification based on scatter statistics would not be straightforward as many different terrains exhibit similar acoustic properties. Additional information such as texture, together with feature detection techniques for faults [13] and seamounts [14] may be incorporated. The prospects for this particular dataset are clearly limited due to the high noise content associated with the poor weather conditions experienced during surveying.

8. REFERENCES

[1] F Aumento, B D Loncarevic & D I Ross, 'IV. Regional studies, Hudson Geotraverse: geology of the Mid-Atlantic ridge at 45°N', *Phil. Trans. Roy. Soc. Lond. A.*, 268 p623-650 (1971)
[2] A S Laughton & R C Searle, 'Tectonic processes on slow spreading ridges', in *Deep drilling results in the Atlantic Ocean: ocean crust*, edited by M. Talwani *et al.*, Washington D.C.: A.G.U. p15-32 (1979)
[3] E Valsami, J R Cann, R C Searle, M Ackers & J A Keeton, 'Morphological characteristics of the Mid-Atlantic ridge at 45°N: implications for magmatic and tectonic processes', *(in prep.)*, (1993)
[4] F Pøhner & E B Lunde, 'Hydrographic applications of interferometric signal processing', *XIX International Congress*, Helsinki, Finland, p404.3/1-404.3/15 (1990)
[5] R J Urick, *Principles of underwater sound*, 3rd edition, McGraw-Hill, New York (1983)
[6] F Pøhner, 'Processing of multibeam echosounder data', *Proc. 3rd Bi. Nat. Ocean Serv. Int. Hydro. Conf.*, p91-101 (1988)
[7] W Smith & P Wessel, 'Gridding with continuous curvtature splines in tension', *Geophysics*, 55 p293-305 (1990)
[8] C M McKinney & C D Anderson, 'Measurements of backscattering of sound from the ocean bottom', *J. Acoust. Soc. Amer.*, 36 p158-163 (1964)
[9] A W Nolle *et al.* 'Acoustical properties of water-filled sands', *J. Acoust. Soc. Amer.*, 35 p1394-1408 (1963)
[10] C de Moustier & D Alexandrou, 'Angular dependence of 12-kHz seafloor acoustic backscatter', *J. Acoust. Soc. Amer.*, 90(1) p522-531 (1991)
[11] N C Mitchell & M Somers, 'Quantitative backscatter measurements with a long-range side-scan sonar', *IEEE J. Oceanic Eng.*, 14 4 p368-374 (1989)
[12] L M Parson *et al.* 'En echelon axial volcanic ridges at the Reykjanes Ridge: a life cycle of volcanism and tectonics, *E.P.S.L. (in press)*
[13] P R Shaw, 'Ridge segmentation, faulting and crustal thickness in the Atlantic Ocean', *Nature*, 358 p490-493 (1992)
[14] J A Keeton and R C Searle, 'Detection of circular seamounts using the Hough transform', *(in prep.)*